



Atmospheric triggering conditions and climatic disposition of landslides in Kyrgyzstan and Tajikistan at the beginning of the 21st century

Xun Wang¹, Marco Otto¹, and Dieter Scherer¹

¹Chair of Climatology, Technische Universität Berlin, Berlin, 12165, Germany

Correspondence: Xun Wang (xun.wang@tu-berlin.de)

Abstract. Landslide is a major natural hazard in Kyrgyzstan and Tajikistan. Knowledge about atmospheric triggering conditions and climatic disposition of landslides in Kyrgyzstan and Tajikistan is limited, even though this topic has already been investigated thoroughly in other parts of the world. In this study, the newly developed, high-resolution High Asia Refined Analysis version 2 (HAR v2) data set generated by dynamical downscaling was combined with historical landslide inventories to analyze atmospheric conditions that initialized landslides in Kyrgyzstan and Tajikistan. The results indicate the crucial role of snowmelt in landslide triggering processes since it contributes to the initialization of 40% of landslide events. Objective thresholds for rainfall, snowmelt, as well as the sum of rainfall and snowmelt (rainfall+snowmelt) were defined. Peak intensity (I_{max}) and accumulated amount (Q) of rainfall+snowmelt events yield the best predictive performance. Mean annual exceedance maps were derived from regional thresholds of $I_{max} = 12.8 \text{ mm d}^{-1}$ and $Q = 17.2 \text{ mm}$ for rainfall+snowmelt. Mean annual exceedance maps depict climatic disposition and have added value in landslide susceptibility mapping. The results reported in this study highlight the potential of dynamical downscaling products generated by regional climate models in landslide prediction.

1 Introduction

Landslide is one of the most severe natural hazards in Kyrgyzstan and Tajikistan. More than 300 big landslides occurred in Kyrgyzstan from 1993 to 2010, causing 256 fatalities and direct economic losses of 2.5 million USD per year (Torgoev et al., 2012). Under global warming, wildfires, glacial retreat, and permafrost degradation are much likely to enhance slope instabilities in mountainous areas (Froude and Petley, 2018; Palmer, 2020), making these regions, including Kyrgyzstan and Tajikistan, more vulnerable to climate change. Landslides are predetermined by static factors, such as slope gradient and aspect, geology, vegetation cover, etc. (Dai et al., 2002). These factors that make slopes prone to failure without actually initiating it are also referred to as dispositions (Zimmermann, 1997). Landslides are triggered by dynamic factors, which are mainly extreme and prolonged rainfall, rapid snowmelt, as well as earthquakes (Wieczorek, 1996).

The majority of landslide research in Kyrgyzstan and Tajikistan focused on characterizing landslide susceptibility, i.e., "where" landslides are prone to occur (e.g., Braun et al., 2015; Saponaro et al., 2015; Havenith et al., 2015b). But little attention is paid to the atmospheric triggering conditions, and our knowledge of "when" landslides are likely to occur is limited



25 in this region. In addition, most landslide susceptibility studies only took non-climatic factors into account or simply applied
annual precipitation as a climatic factor. According Segoni et al. (2018), no rainfall threshold for landslide triggering has been
defined for Kyrgyzstan and Tajikistan yet, even though this topic has already been thoroughly investigated in other parts of the
world with high landslide susceptibility (e.g., Berti et al., 2012; Gariano et al., 2015; Giannecchini et al., 2016; Leonarduzzi
30 et al., 2017). The reasons are twofold. Firstly, although landslide inventories have been developed in this region, e.g., the
Tien Shan Geohazards Database (Havenith et al., 2015a, b) and the multi-temporal landslide inventory from Behling and
Roessner (2020), there is a lack of landslide inventories with the exact date of landslide occurrence. Given the highly dynamic
nature of weather phenomena, at least a daily time stamp of landslide records is required to investigate weather conditions
that trigger landslides. Secondly, there is a lack of atmospheric data. The number of in-situ observation stations in Kyrgyzstan
and Tajikistan decreased sharply in the 1990s due to reduced funding. There are currently eight stations in Kyrgyzstan and
35 26 stations in Tajikistan available from Global Surface Summary of the Day (GSOD), which is a publicly available data
set. These numbers are already significantly below the recommendation of World Meteorological Organization, even for flat
areas (Ilyasov et al., 2013). Despite the sparse distribution, most GSOD stations are located in low-lying valleys and are not
fully representative of the area.

Rainfall is the most common trigger of landslide all over the world (Wieczorek, 1996). Over snow-covered regions, snowmelt
40 is recognized as another common trigger of shallow landslides and debris flows (Wieczorek, 1996; Mostbauer et al., 2018).
In Kyrgyzstan and Tajikistan, more than half of the annual precipitation falls in the form of snow. Snow cover duration over
high mountain ranges in the Tien Shan and the Pamir is more than 200 days per year (Dietz et al., 2014). A large amount of
water stored in snowpacks is released during the melting season. Snowmelt is another important source of water infiltrating
into the soil that increases slope instability. Thus, in Kyrgyzstan and Tajikistan, snowmelt might also play a role in landslide
45 triggering besides rainfall. But snowmelt is not as easy to be observed as rainfall and might often be neglected as a landslide
trigger, especially when co-occurring with rainfall.

There are two main approaches to assess rainfall threshold for landslide triggering. The first approach is physically based
and requires detailed lithological, morphological, and geotechnical information of each landslide event (Guzzetti et al., 2007).
Unfortunately this level of detail is usually restricted to small areas and is not available for the whole of Kyrgyzstan and
50 Tajikistan. The second one is the empirical approach based on historical landslide and rainfall data. The majority of studies
applying this approach relied on rain gauge data to analyze rainfall thresholds (e.g., Berti et al., 2012; Khan et al., 2012; Bui
et al., 2013). However, rain gauge data are point measurements that cannot capture the large spatial heterogeneity of rainfall,
especially over complex terrains. Gridded products can provide continuous data in both space and time and can be used in
detecting atmospheric triggering conditions of landslides.

55 We aim to analyze the atmospheric triggering conditions of landslides and generate climatic disposition maps that con-
tain information on these triggering conditions in Kyrgyzstan and Tajikistan. For this purpose, we combined freely available
atmospheric data with historical landslide events. Atmospheric triggers for each landslides events were determined by the
co-occurrence of landslide and weather events. Properties (mean intensity, peak intensity, accumulated amount) of landslide
triggering events and non-landslide triggering events were compared. Objective thresholds of these properties for different



60 atmospheric triggers (rainfall, snowmelt, and the sum of rainfall and snowmelt) were defined so that they can best separate atmospheric conditions that resulted and did not result in landslides. Finally, we applied the thresholds with the best predictive performance to generate maps of mean annual exceedance. In this way, we can transform the weather-scale triggering conditions into climate-scale disposition (hereafter referred to as "climatic disposition").

The objective of this study is threefold: (1) investigate the role of snowmelt in landslide triggering processes; (2) find
65 appropriate quantities of atmospheric triggers for assessing landslide hazards; (3) characterize climatic disposition in terms of rainfall and snowmelt over Kyrgyzstan and Tajikistan.

The paper is organized as follows: we describe the data and methods used in this study in the following section. Results are presented in section 3 and discussed in 4. Conclusions are drawn in section 5.

2 Data and method

70 2.1 Data

2.1.1 Landslide catalog

Landslide events used in this study come from two sources: the Global Landslide Catalog (GLC) (Kirschbaum et al., 2010, 2015) and the Global Fatal Landslide Database (GFLD) (Froude and Petley, 2018). GLC has been compiled by NASA since 2007 and contains all types of mass movements triggered mostly by rainfall. The sources of the GLC are mainly media reports,
75 disaster databases, and scientific reports. The GFLD only includes landslide events that caused fatality obtained from media reports. It currently covers the period from 2004 to 2017. Both the GLC and the GFLD provide dates of landslide events.

We selected landslide events triggered by atmospheric factors in Kyrgyzstan and Tajikistan from 2007-2018 from the GLC and 2004-2017 from the GFLD. Then we merged these two data sets and deleted duplicated events that occurred on the same day and came from the same source link, resulting in 96 landslide events for Kyrgyzstan and Tajikistan from 2004 to 2018
80 (Fig. 1).

2.1.2 Atmospheric data

Rainfall and snowmelt data are extracted from the HAR v2. The HAR v2 is a newly developed regional atmospheric data set. It was generated by dynamical downscaling of the ERA5 reanalysis data using the Weather Research and Forecasting model (WRF). It is the only gridded atmospheric data set over High Mountain Asia with high resolution and accuracy (Hamm et al.,
85 2020). Detailed modeling strategies of the HAR v2 are described in Wang et al. (2021). The HAR v2 has a grid spacing of 10 km and is available in hourly, daily, monthly and yearly aggregations. Daily products were used in this study to determine the climatic trigger of each landslide event (section 2.2.1) and to define thresholds for landslide triggering (section 2.2.2). Rainfall was calculated as the difference between total precipitation and snowfall. Snowmelt is not a standard output of the WRF and was calculated using the Surface Energy Balance (SEB). The SEB in the HAR v2 is resolved by the Noah Land Surface Model
90 (LSM) (Tewari et al., 2004):



$$H_m = R_n - H_s - H_l - H_g \quad (1)$$

where R_n , H_s , H_l and H_g are net radiation, sensible heat flux, latent heat flux and ground heat flux in W m^{-2} , respectively. These four variables are directly available in the HAR v2. H_m is the heat flux for melting and refreezing in W m^{-2} . $H_m > 0$ indicates melting process, while $H_m < 0$ refers to refreezing process. When $H_m > 0$, snowmelt h_m ($\text{kg m}^{-2} \text{s}^{-1}$) is calculated

95 as:

$$h_m = H_m / \lambda_m \quad (2)$$

where λ_m is the latent heat of fusion. When the calculated h_m is greater than snow water equivalent, then h_m is set to be equal to snow water equivalent.

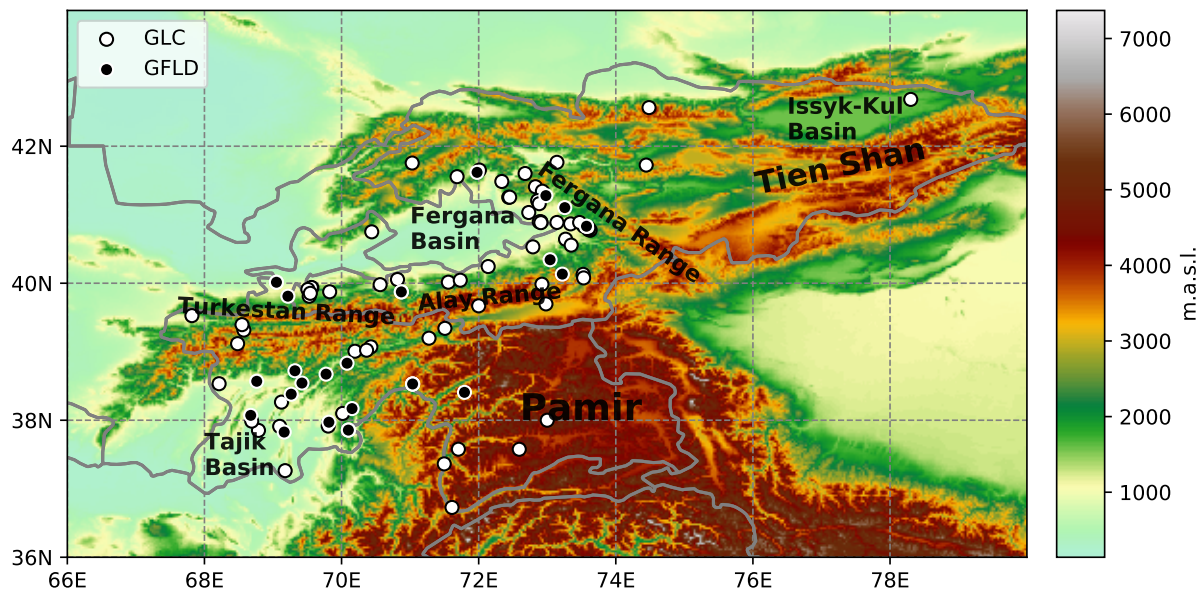


Figure 1. Landslide events from 2004-2018 extracted from the Global Landslide Catalog (GLC) (white points) and the Global Fatal Landslide Database (GFLD) (black points). Background contour is topography from Digital Elevation Model data from Shuttle Radar Topographic Mission.



2.2 Methods

100 2.2.1 Determine atmospheric trigger of landslide events

Atmospheric trigger of a landslide event is determined by the co-occurrence of the landslide event with rainfall and snowmelt event. If a landslide event only occurred within or one day after a rainfall (snowmelt) event, then this landslide event is defined as rainfall (snowmelt) triggered. If there are both a rainfall event and a snowmelt event on the day or one day before the landslide occurrence day, then the atmospheric trigger of this landslide event is mixed.

105 To define a rainfall (snowmelt) event, the daily time series of rainfall(snowmelt) were extracted from the grid cells where landslides occurred. For each time series, an independent event is defined as a series of consecutive days in which more than 0.2 mm d^{-1} of rainfall (snowmelt) is simulated. The value of 0.2 mm d^{-1} is chosen because it is the traditional precision of daily precipitation measurement (Jarraud, 2008) and can be applied to separate dry and wet conditions (Rodwell et al., 2010).

2.2.2 Threshold model for atmospheric triggers

110 The threshold model developed in this study contains three steps: (1) define landslide triggering events and non-triggering events; (2) define the thresholds for rainfall, snowmelt, and the sum of rainfall and snowmelt (hereafter referred to as rainfall+snowmelt) based on maximizing the predictive performance using 2×2 contingency tables; (3) validate and assess the uncertainties of the defined thresholds. The methods for the first two steps were adopted from Leonarduzzi et al. (2017). Only the landslide events, the climatic triggers of which could be determined, were used for threshold modeling.

115 The first step is to define landslide triggering events and non-triggering events for rainfall, snowmelt, and rainfall+snowmelt. Here, we take rainfall as an example to describe the procedure. First, the method used in section 2.2.1 is applied to define rainfall events for each time series extracted from grid cells where landslides occurred. Next, if a landslide event occurred during or one day after a rainfall event, then this rainfall event is classified as a landslide triggering event (LTE). Given the uncertainty in time stamps of landslide events, the day after is also considered as a temporal relaxation. Otherwise, if a rainfall event is not associated with any landslide events, it is classified as a non-landslide triggering event (NLTE). For each rainfall event, we calculated three event properties: mean intensity I_{mean} , maximum intensity I_{max} , and the accumulated amount of rainfall for the entire event Q . For triggering events, we also calculated these three properties by only considering the period up to the day of the landslide occurrence (hereafter referred to as UTL, meaning Up-To-Landslide). Note that, not all the landslide events co-occurred with a rainfall event. For these events, we set I_{mean} , I_{max} , and Q to zero. The same procedure for defining
120 LTEs and NLTEs was conducted for snowmelt and rainfall+snowmelt as well.

The second step is to define thresholds of rainfall, snowmelt, and rainfall+snowmelt for entire events and UTL events, using I_{mean} , I_{max} , and Q . No single threshold can perfectly separate LTEs from NLTEs since their distributions overlap. We applied 2×2 contingency tables to select the threshold that yields the best predictive performance. Using a certain threshold as a binary classifier, LTEs and NLTEs were categorized into true positive (TP), true negative (TN), false positive (FP), and
130 false negative (FN). The Peirce Skill Score (PSS) (Hanssen and Kuipers, 1965) was applied as the measure of the predictive performance because it is trail-independent, which means it is unbiased even when the numbers of LTEs and NLTEs are not



equally presented (Woodcock, 1976). The PSS is also known as the Hanssen-Kuiper skill score and the true skill statistic. It is calculated as the difference between Hit Rate (HR) and False Alarm Rate (FAR):

$$PSS = HR - FAR \quad (3)$$

135

$$HR = \frac{TP}{TP + FN} \quad (4)$$

$$FAR = \frac{FP}{FP + TN} \quad (5)$$

We chose the threshold that maximizes the PSS. We also computed the Euclidean distance (d) to the optimal point (HR=1, FAR=0), which is another commonly used skill score in this application (e.g., Gariano et al., 2015; Piciullo et al., 2017; Postance et al., 2018; Zhuo et al., 2019). Additionally, the receiver operating characteristic (ROC) curve was used to determine the general predictive power of a certain predictor by calculating the area under the ROC curve (AUC) (Fawcett, 2006).

140

The last step is to validate the threshold model and assess uncertainty. For the calibration of thresholds, all landslide event samples were utilized, and corresponding statistic measures were calculated, i.e., the threshold model was trained and tested on the same data set. To test the model's predictive ability on an unseen data set, we performed k-fold cross-validation. Landslide events were randomly split into k folds with k=8. Then for each unique fold, the fold was taken as the testing set, and the remaining k-1 folds were taken as the training set. Mean values of thresholds, the corresponding statistic measures, as well as their uncertainties represented by standard deviations were reported.

145

2.2.3 Mean annual exceedance

Mean annual exceedance (\bar{N}_{th}) is calculated for each HAR v2 grid cell. It is defined as the number of events that exceed a certain threshold over a certain period (N_{th}) divided by the total number of years (N_a):

150

$$\bar{N}_{th} = \frac{N_{th}}{N_a} \quad (6)$$

The unit of \bar{N}_{th} is the number of events per year. Mean annual exceedance transforms weather-scale triggering conditions to climate-scale disposition. It depicts where are landslides likely to occur from climatic aspect.

3 Results

3.1 The role of snowmelt in landslide triggering

155 Fig. 2 shows the climatology of seasonal rainfall, snowmelt, and rainfall+snowmelt resolved by the HAR v2. A high amount of rainfall concentrates in the western foothill of the Fergana Range, the northern foothill of the Turkestan Range, and the Tajik Basin in spring and shifts northeastwards into the Tien Shan in summer. Snowmelt occurs in spring over most high elevated areas. In summer, while most regions are snowmelt-free, the Pamir plateau still experiences a high amount of continuous snowmelt, which is in line with the results by Dietz et al. (2014) using remote sensing data.



160 Atmospheric triggers for each landslide events are determined using the method described in section 2.2.1, and the results
are shown in Fig. 3. Table A1 lists all 96 events and the climatic triggers detected by the HAR v2. Nine landslide events did
not occur within any rainfall event, snowmelt event, or rainfall+snowmelt event. These events are referred to as "not detected"
(white points in Fig. 3) and are excluded. The remaining 87 landslide events were used for further analysis. Landslide events
that were only triggered by rainfall mainly cluster in Tajik Basin and the northeastern rim of the Fergana Basin, where the
165 contribution of rainfall to the annual sum of rainfall and snowmelt is high (Fig. 3).

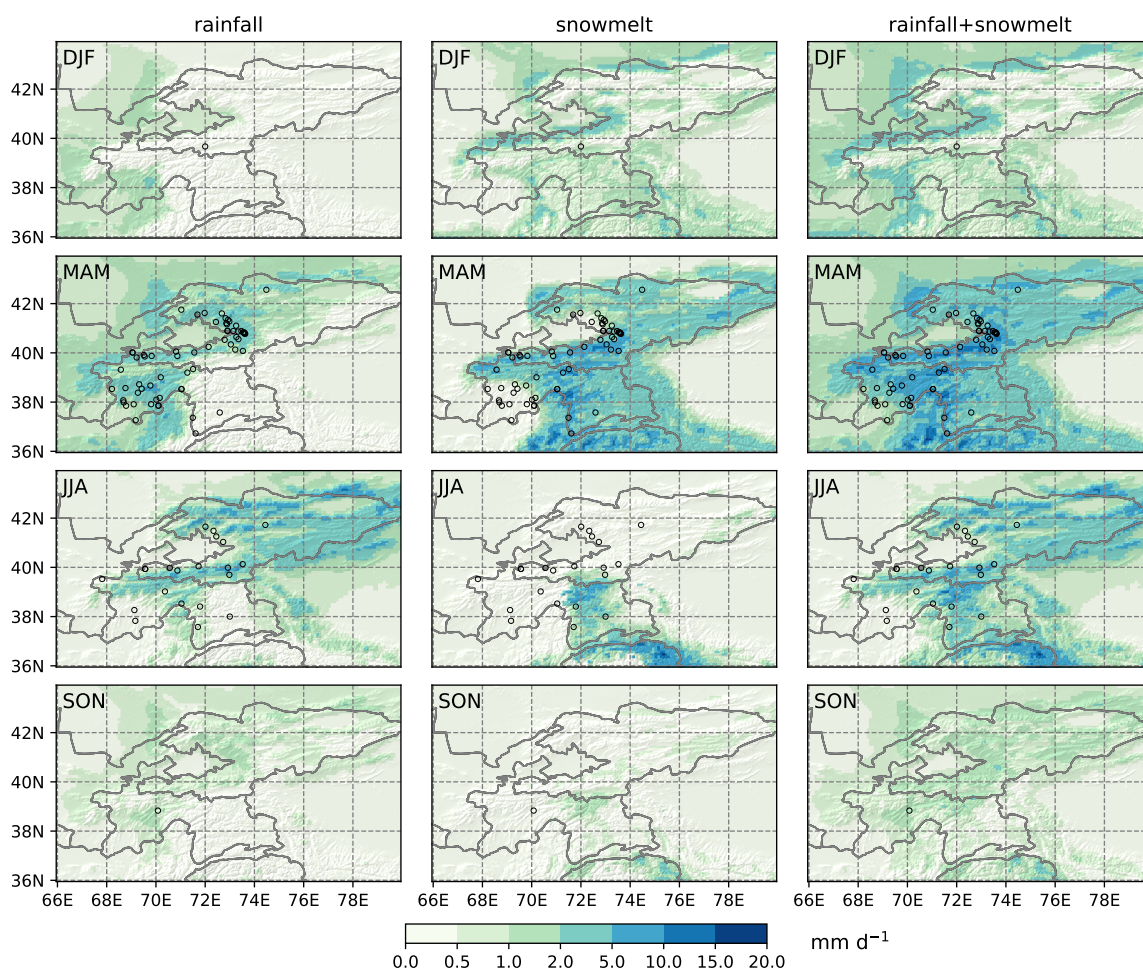


Figure 2. Seasonal rainfall, snowmelt, and rainfall+snowmelt from the High Asia Refined Analysis version 2 (HAR v2) from 2004-2018. Black points: seasonal landslide events from Global Landslide Catalog (GLC) and Global Fatal Landslide Database (GFLD). Topographic shading is based on Digital Elevation Model data from Shuttle Radar Topographic Mission.

The annual cycles of rainfall, snowmelt, and rainfall+snowmelt are compared with monthly landslide occurrences in Fig. 4. The study region experiences a peak of landslide activity in April and May, which corresponds with the peak of rain-



170 fall+snowmelt. While rainfall is the dominant trigger of landslides, snowmelt contributes to triggering 40% of landslide events (35 out of 87). There are 29% of landslide events (25 out of 87) that are attributed to the combined effect of rainfall and snowmelt. Most snowmelt-contributing events occurred in April when snowmelt amount is the highest. March and June have almost the same amount of rainfall+snowmelt. However, there are more landslide occurrences in June. This could be resulted from still frozen soil in March, which stabilizes the slope. As shown in Fig. 4a, both soil temperature at the top soil layer (0-0.1m) and air temperature at 2 m are still zero in March.

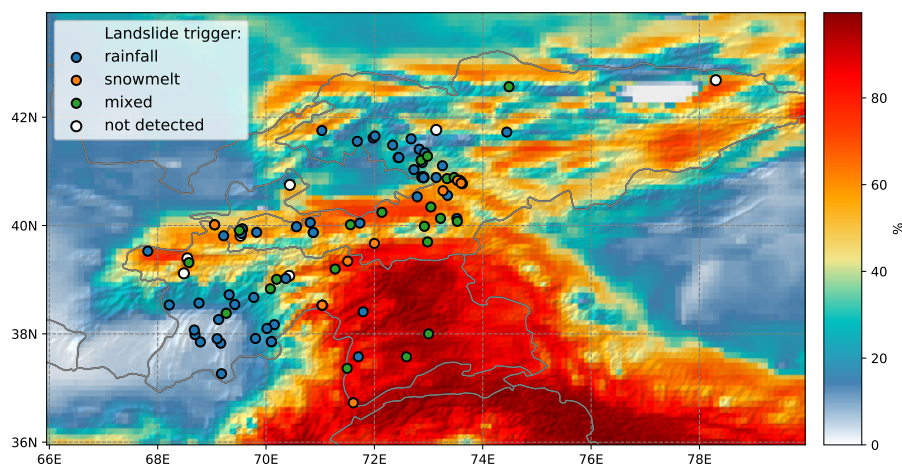


Figure 3. Contribution (%) of snowmelt to annual sum of rainfall and snowmelt (background contour) and climatic triggers of 96 landslide events extracted from Global Landslide Catalog (GLC) and Global Fatal Landslide Database (GFLD) (points). Topographic shading is based on Digital Elevation Model data from Shuttle Radar Topographic Mission.

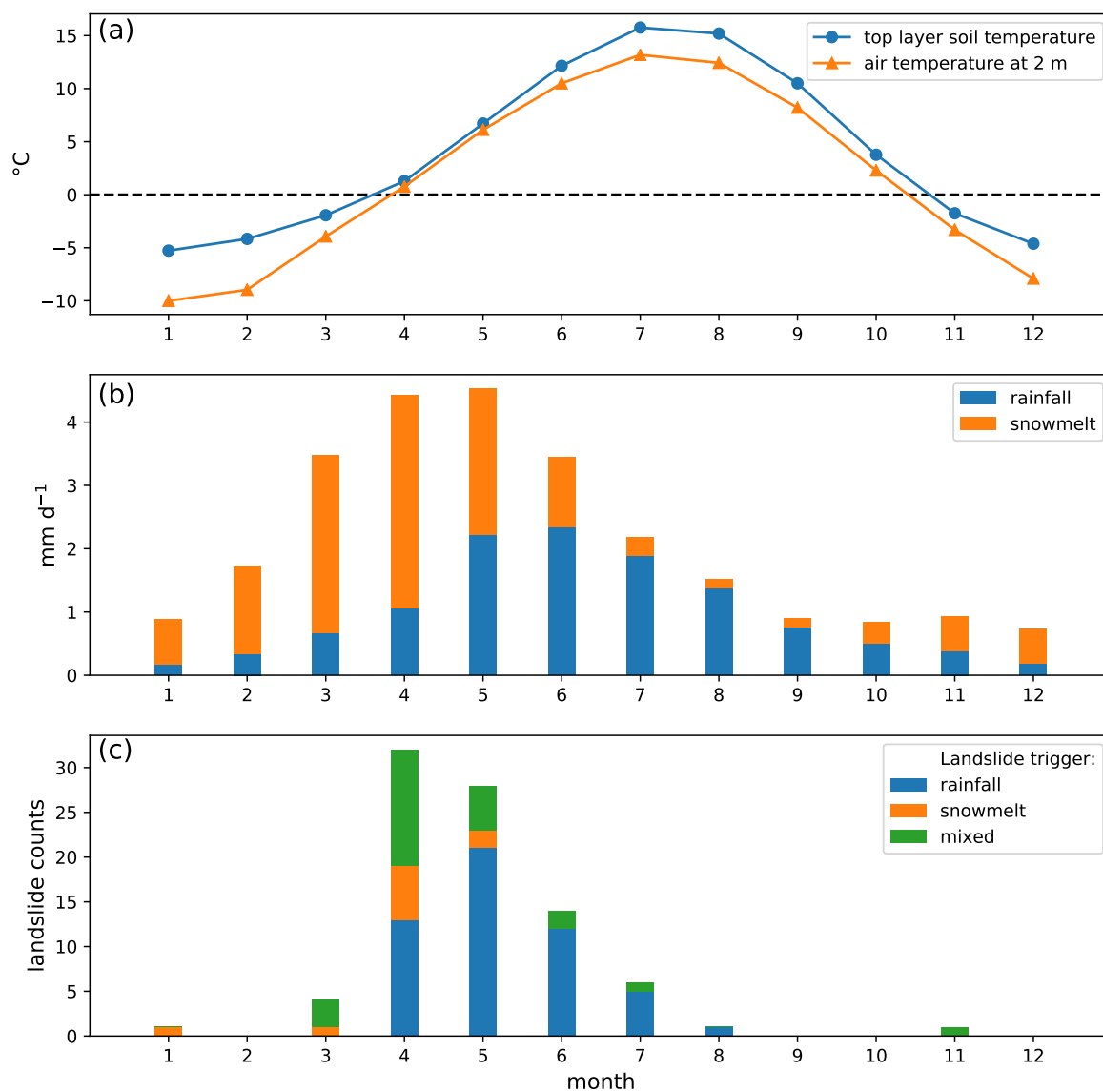


Figure 4. (a) Mean monthly soil temperature at the top soil layer (0-0.1m) and air temperature at 2 m averaged over Kyrgyzstan and Tajikistan extracted from the High Asia Refined Analysis version 2 (HAR v2); (b) mean monthly rainfall and snowmelt averaged over Kyrgyzstan and Tajikistan extracted from the HAR v2; (c) mean monthly landslide occurrences in Kyrgyzstan and Tajikistan from 2004-2018.



3.2 Thresholds of climatic triggers for landslide triggering in Kyrgyzstan and Tajikistan

175 Statistics of different properties of LTEs and NLTEs for rainfall, snowmelt, and rainfall+snowmelt are presented in Fig. 5 in the form of cumulative distribution function (CDF). Rainfall and snowmelt have a high percentage of events with $I_{mean} = 0$, $I_{max} = 0$, and $Q = 0$ because for landslide events that cannot be detected by only rainfall (orange points in Fig. 3) or only snowmelt (blue points in Fig. 3), I_{mean} , I_{max} and Q were all set to zero. It can be seen in Fig. 5 that LTEs, both entire events and UTL events, have stronger I_{mean} and I_{max} , as well as larger Q compared to NLTEs. Besides, snowmelt events have much
180 higher Q but lower I_{mean} and I_{max} than rainfall events, indicating that snowmelt events are in general prolonged and not as intense as rainfall events. Overall, the HAR v2 combined with landslide inventories from GLC and GFLD can distinguish LTEs from NLTEs well and has potential in landslide threshold modeling.

We calibrated thresholds of I_{mean} , I_{max} , and Q using rainfall, snowmelt, and rainfall+snowmelt as predictors. The procedure was conducted for both entire events and UTL events. Predictive performance is better when using the entire period (Table 1)
185 than just using the UTL period (Table A2), which was also concluded by Leonarduzzi et al. (2017). This can also be seen from the CDFs in Fig. 5. In CDF space, the threshold defined by maximizing PPS is the point on the x-axis, where the distance between the LTE curve and the NLTE curve is the largest. CDFs of UTL events are closer to the NLTE curve than CDFs of the entire events. Therefore, the maximum PSSs of UTL events are smaller (Fig. 5). Here, only results for entire events are presented since using the entire period leads to better predictive performance and was mostly used in previous
190 studies (Leonarduzzi et al., 2017). It can be seen from Table 1 that rainfall+snowmelt has the best predictive performance. For rainfall+snowmelt entire event, the best performance is achieved by I_{max} with a threshold value of 12.8 mm d^{-1} , and by Q with a threshold value of 17.2 mm . The PPS and d for I_{max} and Q are very similar, but these two predictors have different advantages. Using I_{max} as predictor leads to a lower FAR but also a lower HR when compared with Q .

K-fold cross-validation results are presented in Table 2. Cross-validation reduces the sample size and makes the results more
195 sensitive to outliers. The validation results are in line with the conclusions drawn by calibration: (1) among all the predictors, rainfall+snowmelt has the best predictive performance; (2) for rainfall+snowmelt entire event, I_{max} and Q are more suitable than I_{mean} ; (3) calibrated thresholds for I_{max} and Q are robust since they fall into the uncertainty range of the thresholds obtained by cross-validation.

3.3 Mean annual exceedance

200 Using the thresholds defined in section 3.2 for rainfall+snowmelt entire event, Fig. 6 presents the annual number of rainfall+snowmelt events that exceed the thresholds of $I_{max} = 12.8 \text{ mm d}^{-1}$ and $Q = 17.2 \text{ mm}$ (hereafter referred to as $I_{max,th}$ and Q_{th}).

Locations with higher mean annual exceedance over $I_{max,th}$ indicate a higher chance of having rainfall + snowmelt event with high intensity, such as the Fergana Range and the northeastern Tajik Basin. These two regions have a high contribution of
205 rainfall to annual rainfall+snowmelt (Fig. 3), and rainfall events tend to have stronger intensity than snowmelt events (Fig. 5). Locations with high mean annual exceedance over Q_{th} but low exceedance over $I_{max,th}$, including the Pamir Plateau and the

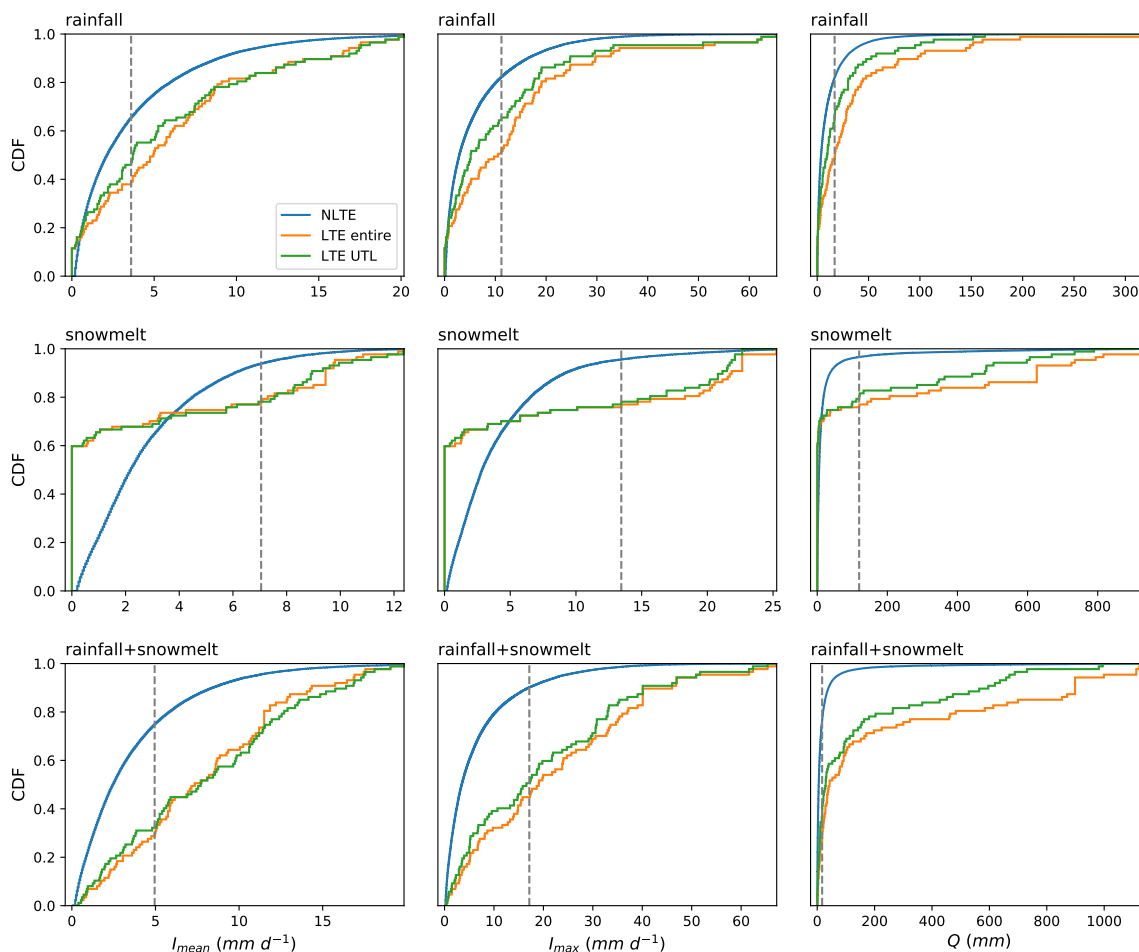


Figure 5. Cumulative distribution function (CDF) curves of mean intensity (I_{mean}), maximum intensity (I_{max}), and accumulated amount (Q) of non-landslide triggering event (NLTE), landslide-triggering entire event (LTE entire), and landslide-triggering up-to-landslide event (LTE UTL) for rainfall, snowmelt, and rainfall+snowmelt during the period of 2004–2018. Grey dashed lines represent the thresholds defined in Table 1.

Tien Shan, indicate that prolonged events instead of short and intense events are more frequent. The mean annual exceedance map of Q_{th} corresponds better with the landslide occurrences since it takes both extreme events and prolonged events into account. Landslide events reported from the GLC and the GFLD are generally located in areas with high exceedance over Q_{th} .
 210 However, the mean annual exceedance map of Q_{th} also has more areas with false alarms, i.e., areas with high mean annual exceedance but no landslide occurrence. In remote areas, such as the Tien Shan, high false alarm could be due to the fact that landslides extracted from median reports are generally under-reported in remote regions. This is discussed in details in section



Table 1. Calibrated thresholds of mean intensity I_{mean} (mm d^{-1}), maximum intensity I_{max} (mm d^{-1}), and accumulated amount Q (mm) for entire events of rainfall, snowmelt, and the sum of rainfall and snowmelt (rainfall+snowmelt), and corresponding performance statistics.

predictor	property	threshold	HR	FAR	d	PSS	AUC
rainfall	I_{mean}	3.60	0.62	0.35	0.51	0.27	0.62
	I_{max}	11.20	0.49	0.18	0.54	0.32	0.65
	Q	16.95	0.52	0.18	0.52	0.34	0.67
snowmelt	I_{mean}	7.05	0.23	0.06	0.77	0.17	0.31
	I_{max}	13.45	0.24	0.04	0.76	0.20	0.32
	Q	119.60	0.24	0.03	0.76	0.21	0.33
rainfall+snowmelt	I_{mean}	4.95	0.71	0.25	0.38	0.46	0.78
	I_{max}	12.80	0.67	0.15	0.37	0.51	0.81
	Q	17.15	0.74	0.23	0.35	0.50	0.81

Table 2. K-fold validation results. Mean values and standard deviations (in parentheses) for thresholds of mean intensity I_{mean} (mm d^{-1}), maximum intensity I_{max} (mm d^{-1}), and accumulated amount Q (mm) for entire events of rainfall, snowmelt, and the sum of rainfall and snowmelt (rainfall+snowmelt), and corresponding performance statistics.

predictor	property	threshold	HR	FAR	d	PSS	AUC
rainfall	I_{mean}	3.76	0.56	0.33	0.56	0.23	0.62
		(0.33)	(0.14)	(0.03)	(0.10)	(0.13)	(0.01)
		11.06	0.46	0.18	0.57	0.28	0.65
	I_{max}	(0.66)	(0.16)	(0.02)	(0.15)	(0.15)	(0.01)
		12.31	0.53	0.25	0.55	0.27	0.67
		(3.88)	(0.16)	(0.07)	(0.10)	(0.10)	(0.01)
snowmelt	I_{mean}	7.06	0.22	0.06	0.78	0.16	0.31
		(0.02)	(0.14)	(0.01)	(0.14)	(0.14)	(0.02)
		13.61	0.23	0.04	0.77	0.19	0.32
	I_{max}	(0.44)	(0.13)	(0.01)	(0.13)	(0.12)	(0.01)
		122.38	0.23	0.03	0.77	0.20	0.33
		(7.93)	(0.13)	(0.01)	(0.13)	(0.12)	(0.01)
rainfall+snowmelt	I_{mean}	4.96	0.70	0.25	0.40	0.45	0.78
		(0.02)	(0.13)	(0.02)	(0.08)	(0.14)	(0.01)
		12.93	0.65	0.15	0.39	0.49	0.81
	I_{max}	(0.37)	(0.15)	(0.01)	(0.13)	(0.15)	(0.01)
		17.20	0.71	0.23	0.38	0.48	0.81
		(0.14)	(0.15)	(0.02)	(0.10)	(0.13)	(0.01)



4.1. In contrast, the mean annual exceedance map of $I_{max,th}$ misses more landslide events but has less false alarm area when compared to the exceedance map of Q_{th} .

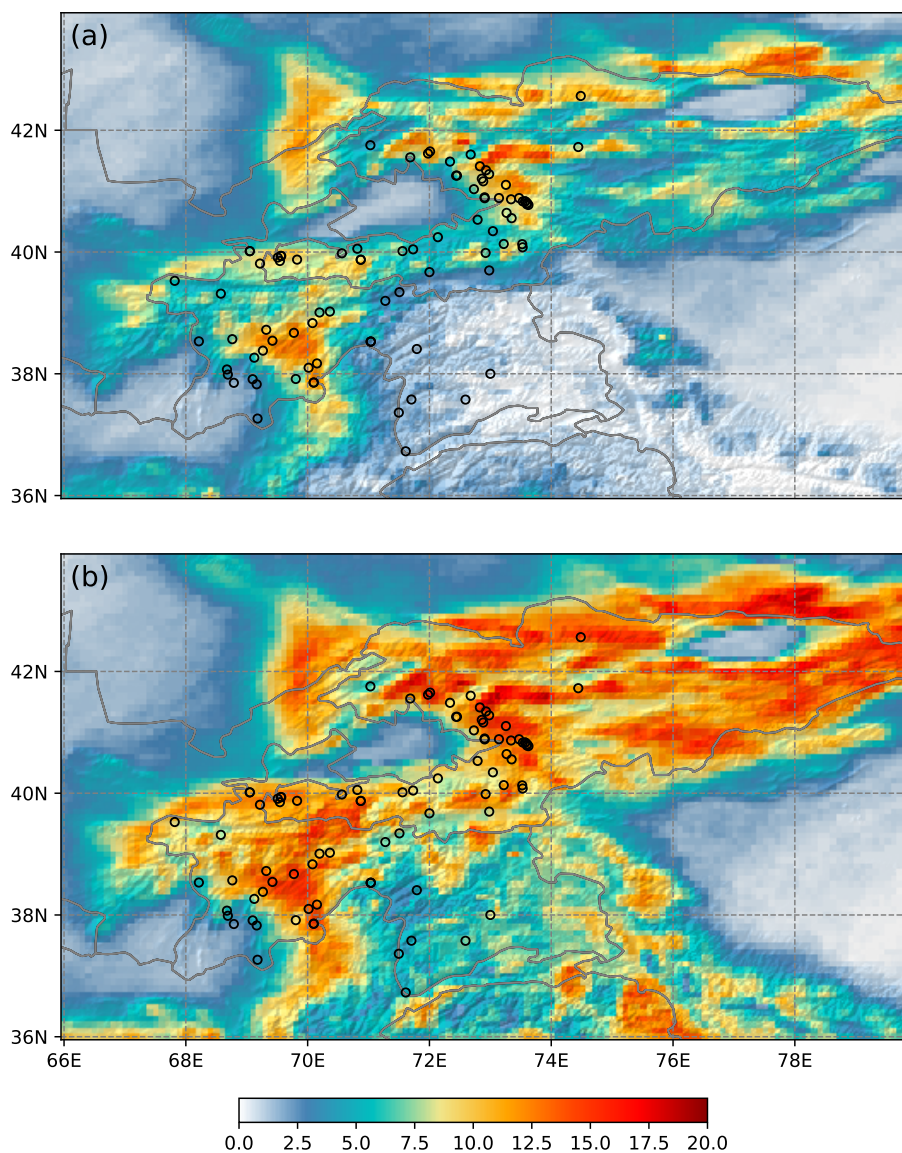


Figure 6. Mean annual exceedance (number of events per year) of (a) $I_{max} = 12.8 \text{ mm d}^{-1}$ and (b) $Q = 17.2 \text{ mm}$ for the sum of rainfall and snowmelt. Black points: landslide events from Global Landslide Catalog (GLC) and Global Fatal Landslide Database (GFLD). Topographic shading is based on Digital Elevation Model data from Shuttle Radar Topographic Mission.



215 4 Discussion

4.1 Sources of uncertainties

Uncertainties of the GLC and GFLD are comprehensively discussed in Kirschbaum et al. (2010), Kirschbaum et al. (2015), and Froude and Petley (2018). The first major problem of these two data sets is that they underestimate the total number of landslides. This is because these two data sets' primary sources are media reports, which are biased towards events with human casualties (Carrara et al., 2003). The second issue is that the spatial distribution of landslides is biased towards populated areas. In our study area, landslide events also tend to cluster in areas with high population density, e.g., the eastern rim of the Fergana Basin and the Tajik Basin. Landslide number over remote areas is much likely to be under-reported. Last but not least, there is large uncertainty in landslide location because most media reports do not contain the exact location where landslides initiated, but rather just the name of the village, road, or city affected by landslides. An example in our case is the landslide event in the Issyk-Kul Basin (Fig. 1), the location of which is in a flat area, and the location accuracy provided by the GLC is "exact". This landslide event's initial zone must be different from the reported location and somewhere nearby with slopes. We also failed to determine the climatic trigger of this landslide event using the HAR v2. Despite these known limitations, the GLC and the GFLD still provide the lower boundary of landslide number and are proven to be valuable in global and regional landslide studies (Kirschbaum and Stanley, 2018; Jia et al., 2020; Stanley et al., 2020). Although the landslide number is known to be incomplete, our results show that they can still present the seasonal distribution of landslide occurrence reasonably well (Fig. 4). This was also concluded by Kirschbaum et al. (2015), who stated that the reason for unbiased seasonal distribution of landslide occurrence is that the compilation method depends on media alerts, which is consistent throughout the year. Additionally, even though location uncertainty exists, we could determine atmospheric triggers of 91% of landslide events (87 out of 96). The reason could be that landslide-triggering rainfall and snowmelt events generally have a large spatial extend (Leonarduzzi et al., 2017).

Another source of uncertainty comes from the rainfall and snowmelt data simulated in the HAR v2. Compared to the old version of the High Asia Refined Analysis (HAR) (Maussion et al., 2014), HAR v2 can simulate precipitation over High Mountain Asia as accurately as the old version. Simulation of air temperature at 2 m is better than the old version due to the snow depth correction approach (Wang et al., 2021). Hamm et al. (2020) compared the HAR v2 with other gridded precipitation data sets, including reanalysis data and satellite-based precipitation retrieval. It was concluded that HAR v2 is the only product that can resolve orographic precipitation, which is a fundamental process over complex terrain. Furthermore, the HAR v2 can capture more extreme precipitation events than coarser products. Snowmelt in the HAR v2 is resolved by the Noah LSM, which only considers a single layer of snowpack (Koren et al., 1999). Several studies found uncertainty of the Noah LSM in reproducing the snow-related process, e.g., the overestimation of snow albedo (e.g., Chen et al., 2014; Minder et al., 2016; Tomasi et al., 2017). Nevertheless, the snow-related process is the major weakness of LSMs and needs further improvement in the future (Chen et al., 2014). Despite the uncertainty in the HAR v2, our results show that it can distinguish LTEs from NLTEs very well (Fig. 5), suggesting that the HAR v2 and dynamical downscaling products, in general, are suitable for extracting weather conditions corresponding to landslides.



Our approach is purely empirical-based, which allows us to investigate broader areas without knowing the detailed surface characteristics of each landslide event. However, slope instability often results from numerous factors. The interaction between non-climatic characteristics and atmospheric triggers is also responsible for the initiation of landslides (Berti et al., 2012; Jia et al., 2020), which can not be captured by empirical methods. This is the reason why not all rainfall+snowmelt events that exceed $I_{max,th}$ and Q_{th} triggered landslides (Fig. 6), even though the number of landslides is underestimated.

4.2 Climatic disposition

In probabilistic risk analysis (e.g., Scherer et al., 2013), the risk that a system experiences an adverse effect caused by a hazardous process is given as the product of hazard and vulnerability. Vulnerability itself depends on exposure and sensitivity. Adverse effects only occur when the elements at risk are exposed to a hazardous event. Thus, risk is a function of hazard, exposure and sensitivity. Applying this risk concept to our case, adverse effect is landslide triggered by rainfall+snowmelt, and hazardous process is rainfall+snowmelt events that exceed $I_{max,th}$ and Q_{th} . The risk that a location experiences landslide triggered by rainfall+snowmelt depends on two factors: (a) how frequent a location is exposed to rainfall+snowmelt events that exceed $I_{max,th}$ and Q_{th} , and (b) how sensitive slope instability can be triggered at this location. Climatic disposition represented by mean annual exceedance is actually factor (a) and comprises both aspects of hazard and exposure. Sensitivity is non-climatic landslide susceptibility that is only controlled by terrestrial characteristics. Thus, to assess landslide susceptibility, both climatic and non-climatic aspects need to be included.

The majority of landslide susceptibility studies only considered non-climatic factors. We compared our mean annual exceedance maps with a non-climatic landslide susceptibility map developed by Stanley and Kirschbaum (2017) at a resolution of approximately 1 km (Fig. 7). This non-climatic susceptibility map was generated using a heuristic fuzzy approach, in which slope, faults, geology, forest loss, and road networks were taken into account. This map is chosen because it covers the whole of Kyrgyzstan and Tajikistan. Even though the non-climatic susceptibility map and our mean annual exceedance maps were generated by totally different methods, they share some similarities. They both show higher values over areas with steep slopes and lower values in intermontane basins and valleys. This is because topographic relief is considered the best first-order rainfall predictor (Bookhagen and Strecker, 2008). The non-climatic susceptibility map includes information on topography, and topography is explicitly resolved during dynamical downscaling. Mean annual exceedance maps not only display these local-scale features caused by topography but also comprise general atmospheric circulation processes. Discrepancies between the landslide susceptibility map and our exceedance maps, e.g., over the Pamir Plateau and the southwestern Tajik Basin, suggest that for landslide susceptibility mapping, both climatic and non-climatic aspects need to be considered.

In addition, some landslide susceptibility studies took climate into account, but they often simply applied averaged annual precipitation (e.g., Shahabi et al., 2014; Havenith et al., 2015b; Wang et al., 2015). Averaged annual precipitation only shows the climatological conditions in general. Mean annual exceedance is derived from weather-scale triggering conditions, and therefore, it also contains information on extreme processes. In our case, for instance, the mean annual rainfall+snowmelt map does not correspond well with landslide occurrences, especially in the Tajik Basin and the northeastern rim of the Fergana



Basin (Fig. 8). But these landslide events are captured better in both mean annual exceedance maps (Fig. 6). This indicates the added value of climatic disposition derived from triggering conditions.

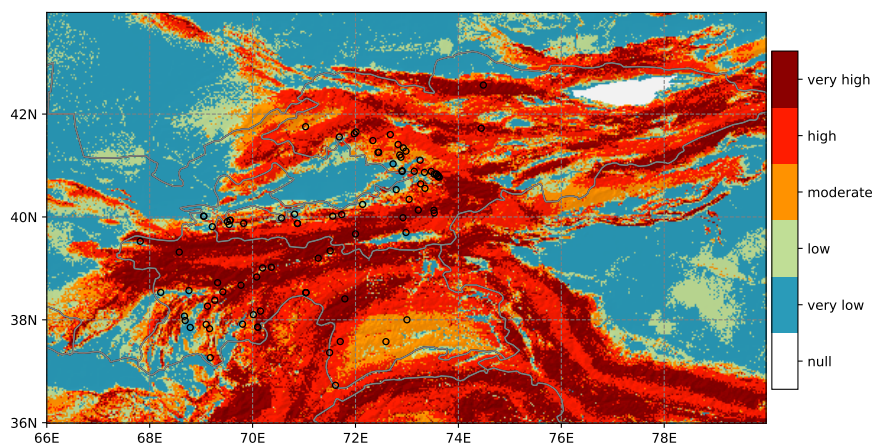


Figure 7. Non-climatic landslide susceptibility map computed using slope, geology, fault zones, road networks, and forest loss developed by Stanley and Kirschbaum (2017). Black points: landslide events from Global Landslide Catalog (GLC) and Global Fatal Landslide Database (GFLD). Topographic shading is based on Digital Elevation Model data from Shuttle Radar Topographic Mission.

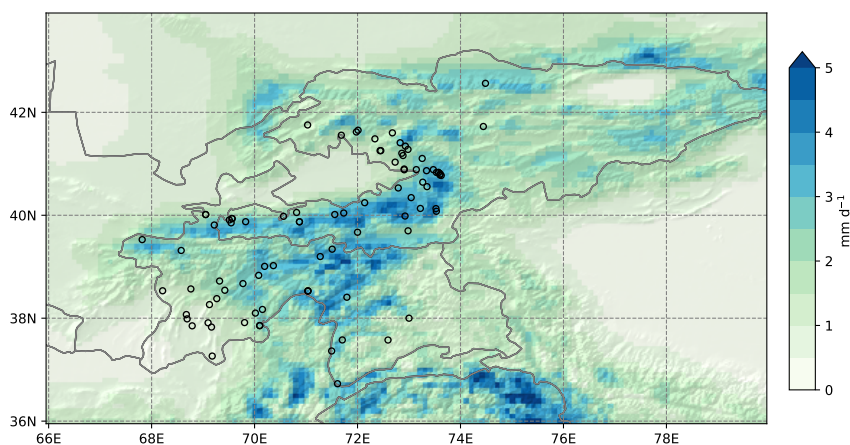


Figure 8. Annual sum of rainfall and snowmelt averaged over 2014-2018 from High Asia Refined Analysis version 2. Black points: landslide events from Global Landslide Catalog (GLC) and Global Fatal Landslide Database (GFLD). Topographic shading is based on Digital Elevation Model data from Shuttle Radar Topographic Mission.



5 Conclusions

285 In this study, we combined gridded atmospheric data from the HAR v2 with 87 landslide records extracted from the GLC and the GFLD to analyze rainfall and snowmelt conditions that triggered landslides in Kyrgyzstan and Tajikistan. Thresholds for landslide triggering were determined for different event properties for rainfall, snowmelt, and rainfall+snowmelt. Mean annual exceedance maps were generated based on the defined thresholds.

Monthly landslide counts in Kyrgyzstan and Tajikistan correspond well with the monthly distribution of rainfall+snowmelt. An exception is March when soil temperature at the top soil layer (0-0.1m) and air temperature at 2 m are both below zero. Investigation the relationship between landslides and soil temperature could be a topic for future studies. Snowmelt plays a crucial role in landslide triggering in Kyrgyzstan and Tajikistan since it contributes to the triggering of 40% of landslide events. By including snowmelt as an additional trigger, the skill of landslide prediction was significantly improved. I_{max} and Q of rainfall+snowmelt entire events have the best predictive performance. Thresholds of $I_{max} = 12.8 \text{ mm d}^{-1}$ (HR=0.67, FAR=0.15) and $Q = 17.2 \text{ mm}$ (HR=0.74, FAR=0.25) were defined for landslide triggering in Kyrgyzstan and Tajikistan. Mean annual exceedance maps derived from these thresholds depict climatic disposition and have added value in landslide susceptibility mapping.

Our study also demonstrates the potential of the Regional Climate Model (RCM) in landslide prediction. Dynamical downscaling products generated by RCMs can provide physically consistent, high-resolution data that is extremely valuable for data scarce areas. Given the global applicability of the dynamical downscaling method and global coverage of the GLC and the GFLD, our approach can also be applied in other regions, as long as the number and quality of landslide records is sufficient. The GLC and the GFLD suffer from under-reporting problem over remote areas, which suggests the need for combination of different methods in landslide detection in remote regions.

Appendix A

Table A1: Landslide events in Kyrgyzstan and Tajikistan extracted from Global Landslide Catalog (GLC) and Global Fatal Landslide Database (GFLD) from 2004 to 2018. Column "trigger" indicates the trigger of landslide events detected by the High Asia Refined Analysis version 2 (HAR v2).

Event date	Source	Longitude	Latitude	Country	Trigger
2004-04-17	GFLD	73.0420	40.3428	Kyrgyzstan	mixed
2004-05-22	GFLD	69.2172	39.8106	Tajikistan	rainfall
2004-06-14	GFLD	70.8718	39.8734	Kyrgyzstan	rainfall
2004-11-17	GFLD	70.0802	38.8324	Tajikistan	mixed
2005-03-13	GFLD	69.0502	40.0141	Tajikistan	mixed
2005-04-09	GFLD	69.2656	38.3801	Tajikistan	mixed
2007-03-25	GLC	70.1951	39.0071	Tajikistan	mixed



2007-04-01	GLC	72.5920	37.5760	Tajikistan	mixed
2007-04-05	GLC	71.6110	36.7270	Tajikistan	snowmelt
2007-04-17	GLC	71.6849	41.5552	Kyrgyzstan	rainfall
2007-04-17	GLC	68.2140	38.5330	Tajikistan	rainfall
2007-04-22	GLC	73.1416	40.8870	Kyrgyzstan	rainfall
2007-06-05	GFLD	69.1633	37.8276	Tajikistan	rainfall
2007-07-21	GLC	73.0000	38.0000	Tajikistan	mixed
2007-07-22	GLC	70.4400	40.7500	Tajikistan	not detected
2007-07-22	GFLD	71.0363	38.5289	Tajikistan	rainfall
2009-04-16	GFLD	71.9767	41.6184	Kyrgyzstan	rainfall
2009-04-21	GLC	68.7882	37.8515	Tajikistan	rainfall
2009-05-05	GFLD	70.1529	38.1701	Tajikistan	rainfall
2009-05-07	GFLD	69.7741	38.6726	Tajikistan	rainfall
2009-05-11	GFLD	71.0363	38.5289	Tajikistan	snowmelt
2009-05-14	GLC	68.6900	37.9867	Tajikistan	rainfall
2009-05-16	GFLD	71.0363	38.5289	Tajikistan	snowmelt
2009-05-20	GFLD	69.3199	38.7221	Tajikistan	rainfall
2010-03-13	GFLD	69.0502	40.0141	Tajikistan	snowmelt
2010-05-07	GLC	69.8054	37.9148	Tajikistan	rainfall
2010-05-07	GFLD	70.0994	37.8560	Tajikistan	rainfall
2010-06-03	GLC	72.9227	39.9854	Kyrgyzstan	mixed
2011-05-11	GLC	72.8282	41.4088	Kyrgyzstan	rainfall
2011-06-12	GLC	69.1238	38.2644	Tajikistan	rainfall
2011-06-12	GLC	69.5667	39.9342	Kyrgyzstan	rainfall
2012-05-12	GLC	70.8159	40.0538	Kyrgyzstan	rainfall
2012-05-13	GFLD	70.8718	39.8734	Kyrgyzstan	rainfall
2013-06-28	GLC	72.0106	41.6518	Kyrgyzstan	rainfall
2014-04-12	GLC	69.0971	37.9107	Tajikistan	rainfall
2014-04-12	GFLD	70.0994	37.8560	Tajikistan	rainfall
2014-04-16	GFLD	68.6749	38.0710	Tajikistan	rainfall
2014-04-26	GFLD	68.7626	38.5685	Tajikistan	rainfall
2015-04-03	GFLD	69.4222	38.5428	Tajikistan	rainfall
2015-05-08	GLC	70.0162	38.0991	Tajikistan	rainfall
2015-05-24	GLC	72.9053	40.8986	Kyrgyzstan	rainfall
2015-05-24	GFLD	73.2559	41.1036	Kyrgyzstan	rainfall



2015-07-10	GLC	70.4275	39.0712	Tajikistan	not detected
2015-07-16	GLC	71.7041	37.5773	Tajikistan	rainfall
2015-07-21	GFLD	71.7929	38.4071	Tajikistan	rainfall
2016-04-26	GLC	72.9071	40.8894	Kyrgyzstan	not detected
2016-05-09	GLC	68.5748	39.3160	Tajikistan	mixed
2016-05-15	GLC	72.9293	41.3431	Kyrgyzstan	rainfall
2016-05-23	GLC	72.7907	40.5304	Kyrgyzstan	rainfall
2016-05-27	GLC	69.8266	39.8751	Kyrgyzstan	rainfall
2016-05-28	GLC	71.5577	40.0150	Kyrgyzstan	mixed
2016-06-16	GLC	72.3374	41.4850	Kyrgyzstan	rainfall
2016-06-20	GLC	73.5233	40.1293	Kyrgyzstan	rainfall
2016-06-27	GLC	74.4438	41.7246	Kyrgyzstan	rainfall
2016-06-29	GLC	73.1415	41.7649	Kyrgyzstan	not detected
2016-07-29	GLC	69.5597	39.9377	Kyrgyzstan	rainfall
2016-08-16	GLC	78.3019	42.6831	Kyrgyzstan	not detected
2016-08-18	GLC	70.5626	39.9790	Tajikistan	rainfall
2017-01-04	GLC	71.9999	39.6699	Kyrgyzstan	snowmelt
2017-01-26	GLC	72.8834	40.8960	Kyrgyzstan	not detected
2017-03-26	GFLD	73.5725	40.8316	Kyrgyzstan	mixed
2017-04-07	GLC	73.6257	40.7733	Kyrgyzstan	snowmelt
2017-04-09	GLC	73.5335	40.8320	Kyrgyzstan	snowmelt
2017-04-10	GLC	69.5091	39.9095	Kyrgyzstan	mixed
2017-04-11	GLC	72.8601	41.2047	Kyrgyzstan	mixed
2017-04-14	GFLD	73.5725	40.8316	Kyrgyzstan	mixed
2017-04-16	GLC	73.2668	40.6430	Kyrgyzstan	snowmelt
2017-04-16	GLC	73.6000	40.7836	Kyrgyzstan	snowmelt
2017-04-17	GLC	73.6047	40.8044	Kyrgyzstan	mixed
2017-04-18	GLC	71.4973	37.3628	Tajikistan	mixed
2017-04-18	GLC	72.9069	40.8838	Kyrgyzstan	rainfall
2017-04-22	GLC	73.3402	40.8663	Kyrgyzstan	mixed
2017-04-23	GLC	71.5074	39.3410	Tajikistan	snowmelt
2017-04-23	GLC	72.8835	41.1610	Kyrgyzstan	rainfall
2017-04-23	GFLD	72.9801	41.2790	Kyrgyzstan	mixed
2017-04-29	GLC	73.4724	40.8864	Kyrgyzstan	mixed
2017-04-29	GFLD	73.2203	40.1325	Kyrgyzstan	mixed



2017-04-30	GLC	72.4381	41.2550	Kyrgyzstan	rainfall
2017-04-30	GLC	73.5310	40.0774	Kyrgyzstan	mixed
2017-05-10	GLC	74.4847	42.5635	Kyrgyzstan	mixed
2017-05-11	GLC	73.3497	40.5560	Kyrgyzstan	rainfall
2017-05-16	GLC	71.0302	41.7545	Kyrgyzstan	rainfall
2017-05-17	GLC	72.6771	41.6014	Kyrgyzstan	rainfall
2017-05-28	GLC	71.2755	39.1978	Tajikistan	mixed
2017-06-19	GLC	72.9814	39.6978	Kyrgyzstan	mixed
2017-06-19	GLC	71.7318	40.0439	Kyrgyzstan	rainfall
2017-06-26	GLC	67.8173	39.5267	Tajikistan	rainfall
2017-06-28	GLC	68.5480	39.3951	Tajikistan	not detected
2017-06-29	GLC	72.7303	41.0321	Kyrgyzstan	rainfall
2017-06-29	GLC	72.4521	41.2557	Kyrgyzstan	rainfall
2017-07-03	GLC	70.3650	39.0219	Tajikistan	rainfall
2017-07-03	GLC	68.4838	39.1172	Tajikistan	not detected
2017-07-04	GLC	69.5279	39.8102	Kyrgyzstan	not detected
2018-05-13	GLC	69.5445	39.8526	Kyrgyzstan	rainfall
2018-05-16	GLC	69.1773	37.2642	Tajikistan	rainfall
2018-05-21	GLC	72.1386	40.2437	Kyrgyzstan	mixed

Table A2. Calibrated thresholds of mean intensity I_{mean} (mm d^{-1}), maximum intensity I_{max} (mm d^{-1}), and the accumulated amount Q (mm) for up-to-landslide (UTL) events of rainfall, snowmelt and the sum of rainfall and snowmelt (rainfall+snowmelt), and corresponding performance statistics.

predictor	property	threshold	HR	FAR	d	PSS	AUC
rainfall	I_{mean}	3.05	0.60	0.40	0.57	0.20	0.59
	I_{max}	12.40	0.34	0.16	0.67	0.19	0.58
	Q	9.25	0.52	0.31	0.57	0.21	0.59
snowmelt	I_{mean}	7.40	0.22	0.05	0.78	0.17	0.31
	I_{max}	12.80	0.24	0.05	0.76	0.19	0.32
	Q	98.30	0.24	0.04	0.76	0.20	0.32
rainfall+snowmelt	I_{mean}	5.05	0.68	0.25	0.41	0.43	0.76
	I_{max}	14.05	0.59	0.14	0.44	0.45	0.77
	Q	15.56	0.66	0.25	0.43	0.40	0.76



305 *Code and data availability.* The landslide data and atmospheric data used in this study are freely available from the following links:

- Global Landslide Catalog (GLC): <https://maps.nccs.nasa.gov/arcgis/home/item.html?id=eec7aee8d2e040c7b8d3ee5fd0e0d7b9>
- Global Fatal Landslide Database (GFLD): <https://blogs.agu.org/landslideblog/2019/06/18/global-fatal-landslide-database-1/>
- High Asia Refined Analysis version 2 (HAR v2): <https://www.klima.tu-berlin.de/HARv2>

The source code used in this study is freely available upon request.

310 *Author contributions.* All authors were involved in study conceptualization and writing of the manuscript. XW collected the data, carried out the analyses, and produced the visualizations.

Competing interests. The authors declare that they have no conflict of interest

Acknowledgements. This work was supported by the German Federal Ministry of Education and Research (BMBF) under the framework of the “Climatic and Tectonic Natural Hazards in Central Asia (CaTeNA)” project (Grant Number FKZ 03G0878G).



315 References

- Behling, R. and Roessner, S.: Multi-temporal landslide inventory for a study area in Southern Kyrgyzstan derived from RapidEye satellite time series data (2009-2013), 2020.
- Berti, M., Martina, M., Franceschini, S., Pignone, S., Simoni, A., and Pizziolo, M.: Probabilistic rainfall thresholds for landslide occurrence using a Bayesian approach, *Journal of Geophysical Research: Earth Surface*, 117, 2012.
- 320 Bookhagen, B. and Strecker, M. R.: Orographic barriers, high-resolution TRMM rainfall, and relief variations along the eastern Andes, *Geophysical Research Letters*, 35, 2008.
- Braun, A., Fernandez-Steeger, T., Havenith, H.-B., and Torgoev, A.: Landslide Susceptibility Mapping with Data Mining Methods—a Case Study from Maily-Say, Kyrgyzstan, in: *Engineering Geology for Society and Territory-Volume 2*, pp. 995–998, Springer, 2015.
- Bui, D. T., Pradhan, B., Lofman, O., Revhaug, I., and Dick, Ø. B.: Regional prediction of landslide hazard using probability analysis of
325 intense rainfall in the Hoa Binh province, Vietnam, *Natural hazards*, 66, 707–730, 2013.
- Carrara, A., Crosta, G., and Frattini, P.: Geomorphological and historical data in assessing landslide hazard, *Earth Surface Processes and Landforms: The Journal of the British Geomorphological Research Group*, 28, 1125–1142, 2003.
- Chen, F., Barlage, M., Tewari, M., Rasmussen, R., Jin, J., Lettenmaier, D., Livneh, B., Lin, C., Miguez-Macho, G., Niu, G.-Y., et al.: Modeling seasonal snowpack evolution in the complex terrain and forested Colorado Headwaters region: A model intercomparison study, *Journal of*
330 *Geophysical Research: Atmospheres*, 119, 13–795, 2014.
- Dai, F., Lee, C., and Ngai, Y. Y.: Landslide risk assessment and management: an overview, *Engineering geology*, 64, 65–87, 2002.
- Dietz, A. J., Conrad, C., Kuenzer, C., Gesell, G., and Dech, S.: Identifying changing snow cover characteristics in central Asia between 1986 and 2014 from remote sensing data, *Remote Sensing*, 6, 12 752–12 775, 2014.
- Fawcett, T.: An introduction to ROC analysis, *Pattern recognition letters*, 27, 861–874, 2006.
- 335 Froude, M. J. and Petley, D. N.: Global fatal landslide occurrence from 2004 to 2016, *Natural Hazards and Earth System Sciences*, 18, 2161–2181, 2018.
- Gariano, S. L., Brunetti, M. T., Iovine, G., Melillo, M., Peruccacci, S., Terranova, O., Vennari, C., and Guzzetti, F.: Calibration and validation of rainfall thresholds for shallow landslide forecasting in Sicily, southern Italy, *Geomorphology*, 228, 653–665, 2015.
- Giannecchini, R., Galanti, Y., Avanzi, G. D., and Barsanti, M.: Probabilistic rainfall thresholds for triggering debris flows in a human-modified
340 landscape, *Geomorphology*, 257, 94–107, 2016.
- Guzzetti, F., Peruccacci, S., Rossi, M., and Stark, C. P.: Rainfall thresholds for the initiation of landslides in central and southern Europe, *Meteorology and atmospheric physics*, 98, 239–267, 2007.
- Hamm, A., Arndt, A., Kolbe, C., Wang, X., Thies, B., Boyko, O., Reggiani, P., Scherer, D., Bendix, J., and Schneider, C.: Intercomparison of Gridded Precipitation Datasets over a Sub-Region of the Central Himalaya and the Southwestern Tibetan Plateau, *Water*, 12, 3271, 2020.
- 345 Hanssen, A. and Kuipers, W.: ON THE RELATIONSHIP BETWEEN THE FREQUENCY OF RAIN AND VARIOUS METEOROLOGICAL PARAMETERS.(WITH REFERENCE TO THE PROBLEM OF OBJECTIVE FORECASTING)., Koninklijk Nederlands Meteorologisch Instituut, 1965.
- Havenith, H.-B., Strom, A., Torgoev, I., Torgoev, A., Lamair, L., Ischuk, A., and Abdrakhmatov, K.: Tien Shan geohazards database: Earthquakes and landslides, *Geomorphology*, 249, 16–31, 2015a.
- 350 Havenith, H.-B., Torgoev, A., Schlögel, R., Braun, A., Torgoev, I., and Ischuk, A.: Tien Shan geohazards database: Landslide susceptibility analysis, *Geomorphology*, 249, 32–43, 2015b.



- Ilyasov, S., Zabenko, O., Gaydamak, N., Kirilenko, A., Myrsaliev, N., Shevchenko, V., and Penkina, L.: Climate profile of the Kyrgyz Republic, The State Agency for Environmental Protection and Forestry under the Government of the Kyrgyz Republic and The United Nations Development Programme: Bishkek, Kyrgyzstan, 2013.
- 355 Jarraud, M.: Guide to meteorological instruments and methods of observation (WMO-No. 8), World Meteorological Organisation: Geneva, Switzerland, 29, 2008.
- Jia, G., Tang, Q., and Xu, X.: Evaluating the performances of satellite-based rainfall data for global rainfall-induced landslide warnings, *Landslides*, 17, 283–299, 2020.
- Khan, Y. A., Lateh, H., Baten, M. A., and Kamil, A. A.: Critical antecedent rainfall conditions for shallow landslides in Chittagong City of Bangladesh, *Environmental Earth Sciences*, 67, 97–106, 2012.
- 360 Kirschbaum, D. and Stanley, T.: Satellite-based assessment of rainfall-triggered landslide hazard for situational awareness, *Earth's future*, 6, 505–523, 2018.
- Kirschbaum, D., Stanley, T., and Zhou, Y.: Spatial and temporal analysis of a global landslide catalog, *Geomorphology*, 249, 4–15, 2015.
- Kirschbaum, D. B., Adler, R., Hong, Y., Hill, S., and Lerner-Lam, A.: A global landslide catalog for hazard applications: method, results, and limitations, *Natural Hazards*, 52, 561–575, 2010.
- 365 Koren, V., Schaake, J., Mitchell, K., Duan, Q.-Y., Chen, F., and Baker, J.: A parameterization of snowpack and frozen ground intended for NCEP weather and climate models, *Journal of Geophysical Research: Atmospheres*, 104, 19 569–19 585, 1999.
- Leonarduzzi, E., Molnar, P., and McArdell, B. W.: Predictive performance of rainfall thresholds for shallow landslides in Switzerland from gridded daily data, *Water Resources Research*, 53, 6612–6625, 2017.
- 370 Maussion, F., Scherer, D., Mölg, T., Collier, E., Curio, J., and Finkelnburg, R.: Precipitation seasonality and variability over the Tibetan Plateau as resolved by the High Asia Reanalysis, *Journal of Climate*, 27, 1910–1927, 2014.
- Minder, J. R., Letcher, T. W., and Skiles, S. M.: An evaluation of high-resolution regional climate model simulations of snow cover and albedo over the Rocky Mountains, with implications for the simulated snow-albedo feedback, *Journal of Geophysical Research: Atmospheres*, 121, 9069–9088, 2016.
- 375 Mostbauer, K., Kaitna, R., Prenner, D., and Hrachowitz, M.: The temporally varying roles of rainfall, snowmelt and soil moisture for debris flow initiation in a snow-dominated system, *Hydrol. Earth Syst. Sci*, 22, 3493–3513, 2018.
- Palmer, J.: A slippery slope: Could climate change lead to more landslides?, *Eos*, 101, <https://doi.org/10.1029/2020EO151418>, published on 23 November 2020, 2020.
- Piciullo, L., Gariano, S. L., Melillo, M., Brunetti, M. T., Peruccacci, S., Guzzetti, F., and Calvello, M.: Definition and performance of a threshold-based regional early warning model for rainfall-induced landslides, *Landslides*, 14, 995–1008, 2017.
- 380 Postance, B., Hillier, J., Dijkstra, T., and Dixon, N.: Comparing threshold definition techniques for rainfall-induced landslides: A national assessment using radar rainfall, *Earth Surface Processes and Landforms*, 43, 553–560, 2018.
- Rodwell, M. J., Richardson, D. S., Hewson, T. D., and Haiden, T.: A new equitable score suitable for verifying precipitation in numerical weather prediction, *Quarterly Journal of the Royal Meteorological Society*, 136, 1344–1363, 2010.
- 385 Saponaro, A., Pilz, M., Wieland, M., Bindi, D., Moldobekov, B., and Parolai, S.: Landslide susceptibility analysis in data-scarce regions: the case of Kyrgyzstan, *Bulletin of Engineering Geology and the Environment*, 74, 1117–1136, 2015.
- Scherer, D., Fehrenbach, U., Lakes, T., Lauf, S., Meier, F., and Schuster, C.: Quantification of heat-stress related mortality hazard, vulnerability and risk in Berlin, Germany, *DIE ERDE–Journal of the Geographical Society of Berlin*, 144, 238–259, 2013.



- Segoni, S., Piciullo, L., and Gariano, S. L.: A review of the recent literature on rainfall thresholds for landslide occurrence, *Landslides*, 15, 1483–1501, 2018.
- 390 Shahabi, H., Khezri, S., Ahmad, B. B., and Hashim, M.: Landslide susceptibility mapping at central Zab basin, Iran: A comparison between analytical hierarchy process, frequency ratio and logistic regression models, *Catena*, 115, 55–70, 2014.
- Stanley, T. and Kirschbaum, D. B.: A heuristic approach to global landslide susceptibility mapping, *Natural hazards*, 87, 145–164, 2017.
- Stanley, T., Kirschbaum, D. B., Pascale, S., and Kapnick, S.: Extreme Precipitation in the Himalayan Landslide Hotspot, in: *Satellite Precipitation Measurement*, pp. 1087–1111, Springer, 2020.
- 395 Tewari, M., Chen, F., Wang, W., Dudhia, J., LeMone, M., Mitchell, K., Ek, M., Gayno, G., Wegiel, J., and Cuenca, R.: Implementation and verification of the unified NOAH land surface model in the WRF model, in: *20th conference on weather analysis and forecasting/16th conference on numerical weather prediction*, vol. 1115, pp. 2165–2170, American Meteorological Society Seattle, WA, 2004.
- Tomasi, E., Giovannini, L., Zardi, D., and de Franceschi, M.: Optimization of Noah and Noah_MP WRF land surface schemes in snow-melting conditions over complex terrain, *Monthly Weather Review*, 145, 4727–4745, 2017.
- 400 Torgoev, I., Alioshin, Y. G., and Torgoev, A.: Monitoring landslides in Kyrgyzstan., *FOG-Freiberg Online Geoscience*, 33, 2012.
- Wang, Q., Wang, D., Huang, Y., Wang, Z., Zhang, L., Guo, Q., Chen, W., Chen, W., and Sang, M.: Landslide susceptibility mapping based on selected optimal combination of landslide predisposing factors in a large catchment, *Sustainability*, 7, 16 653–16 669, 2015.
- Wang, X., Tolsdorf, V., Otto, M., and Scherer, D.: WRF-based Dynamical Downscaling of ERA5 Reanalysis Data for High Mountain Asia: Towards a New Version of the High Asia Refined Analysis, *International Journal of Climatology*, 41, 743–762, 2021.
- 405 Wieczorek, G. F.: Landslides: investigation and mitigation. Chapter 4-Landslide triggering mechanisms, *Transportation Research Board Special Report*, 1996.
- Woodcock, F.: The evaluation of yes/no forecasts for scientific and administrative purposes, *Monthly Weather Review*, 104, 1209–1214, 1976.
- 410 Zhuo, L., Dai, Q., Han, D., Chen, N., and Zhao, B.: Assessment of simulated soil moisture from WRF Noah, Noah-MP, and CLM land surface schemes for landslide hazard application, *Hydrology and Earth System Sciences*, 23, 4199–4218, 2019.
- Zimmermann, M.: *Murganggefahr und Klimaänderung-ein GIS-basierter Ansatz*, vdf Hochschulverlag AG, 1997.